ACS OMEGA

Open Access

http://pubs.acs.org/journal/acsodf

Article

Hydrangea-like AuPtRu/ZnO-rGO Nanocomposites with Enhanced Peroxidase Mimiking Activity for Senitive Colorimetric Determination of H_2O_2

Jie Dong, Laixi Zhang, Wei Li, Xin Hu, Anyi Chen, and Chaorui Li*

Cite This: *ACS Omega* 2023, 8, 49218−49227

Read Online

ACCESS | Metrics & More | Article Recommendations | Supporting Information

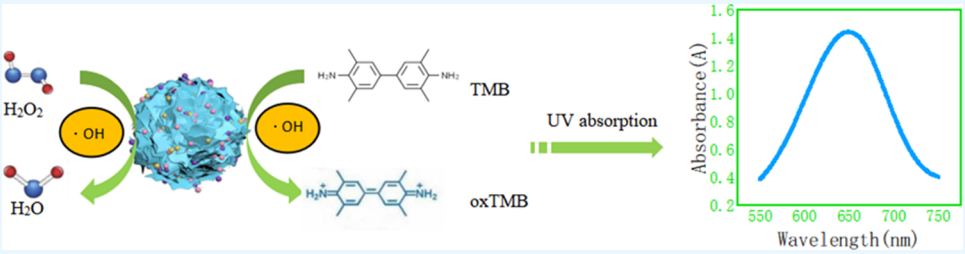

ABSTRACT: In this study, a facile and cost-effective hydrothermal synthesis method was used to synthesize zinc oxide nanoflowers modified by reduced graphene oxide, and subsequently, trimetallic AuPtRu nanoparticles(AuPtRuNPs) were supported via the reduction method for high-sensitivity colorimetric detection of H_2O_2 in weakly acidic solutions. Compared to monometallic and bimetallic nanoparticles, trimetallic nanoparticles exhibit significant synergistic effects and enhanced catalytic activity. After providing a three-dimensional structure with multiple pores by zinc oxide and enhancing electron transfer ability by reduced graphene, the trimetallic nanocomposites (AuPtRu/ZnO-rGO) exhibited excellent peroxidase-mimicking activity, which can effectively catalyze 3,3′,5,5′-tetramethylbenzidine (TMB) to produce a blue oxidation product (oxTMB) in the presence of H_2O_2. Compared to horseradish peroxidase (HRP), AuPtRu/ZnO-rGO demonstrated significantly enhanced catalytic velocity ($V_{max} = 6.16 \times 10^{-8}$ M/s) and affinity ($K_m = 0.02$) for H_2O_2. The study of the catalytic mechanism showed that trimetallic Au, Pt, and Ru could effectively catalyze H_2O_2 to produce hydroxyl radicals ($^{\bullet}OH$) to accelerate the oxidation of TMB and enhance the peroxidase-mimicking activity of the AuPtRu/ZnO-rGO nanocomposites. The results showed that the as-synthesized hydrangea-like AuPtRu/ZnO-rGO nanocomposites showed enhanced peroxidase-mimicking activity. It could be used for the colorimetric detection of H_2O_2 in the range 5−1000 μM with a LOD of 3.0 μM (S/N = 3), and the recoveries are 93.0−101.7%. In addition, the AuPtRu/ZnO-rGO nanocomposites have good applicability for sensitive colorimetric determination of H_2O_2 in milk, and it has broad application prospects as a multifunctional sensing platform in the food processing industry.

1. INTRODUCTION

Hydrogen peroxide (H_2O_2) is a vital molecule in biological tissues, with its concentration playing a crucial role in maintaining physiological balance. However, abnormal levels of H_2O_2 can lead to various physiological diseases including myocardial infarction, Alzheimer's disease, Parkinson's disease, cancer, etc.[1] Additionally, H_2O_2 can be decomposed and generate reactive oxygen species (ROS), which possess antimicrobial properties and can effectively eliminate bacterial spores and active components of bacterial cells.[2,3] Therefore, H_2O_2 is frequently utilized as a bactericide and disinfectant in the food industry to ensure food safety,[4] but excessive or improper use of H_2O_2 will cause harm to the human body and lead to the onset of various diseases. Many countries have established stringent regulations regarding H_2O_2 residues in food. The US Food and Drug Administration (FDA) stipulates that the residual amount of H_2O_2 in the final product cannot exceed 0.5 mg/L. In Japan, H_2O_2 in food must be decomposed or removed before production, and H_2O_2 can be used in only a small part of food production. Moreover, the use of H_2O_2 in the production of dairy products is clearly prohibited in China. Consequently, it is essential to develop a rapid and sensitive method for detecting H_2O_2.

Since Gao et al.[5] discovered that Fe_3O_4 nanoparticles have peroxidase-mimicking activity in 2007, an increasing number of nanomaterials have been synthesized and utilized in the detection of H_2O_2. Therefore, a nanoenzyme with a high catalytic activity similar to that of peroxidase has been developed to replace natural enzymes for H_2O_2 detection,

Received: September 28, 2023
Revised: November 22, 2023
Accepted: November 29, 2023
Published: December 11, 2023

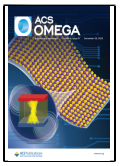

Scheme 1. (A) Schematic Diagram for the Preparation of Hydrangea-like AuPtRu/ZnO-rGO. (B) Schematic Illustration of Hydrangea-like AuPtRu/ZnO-rGO for the Detection of H_2O_2

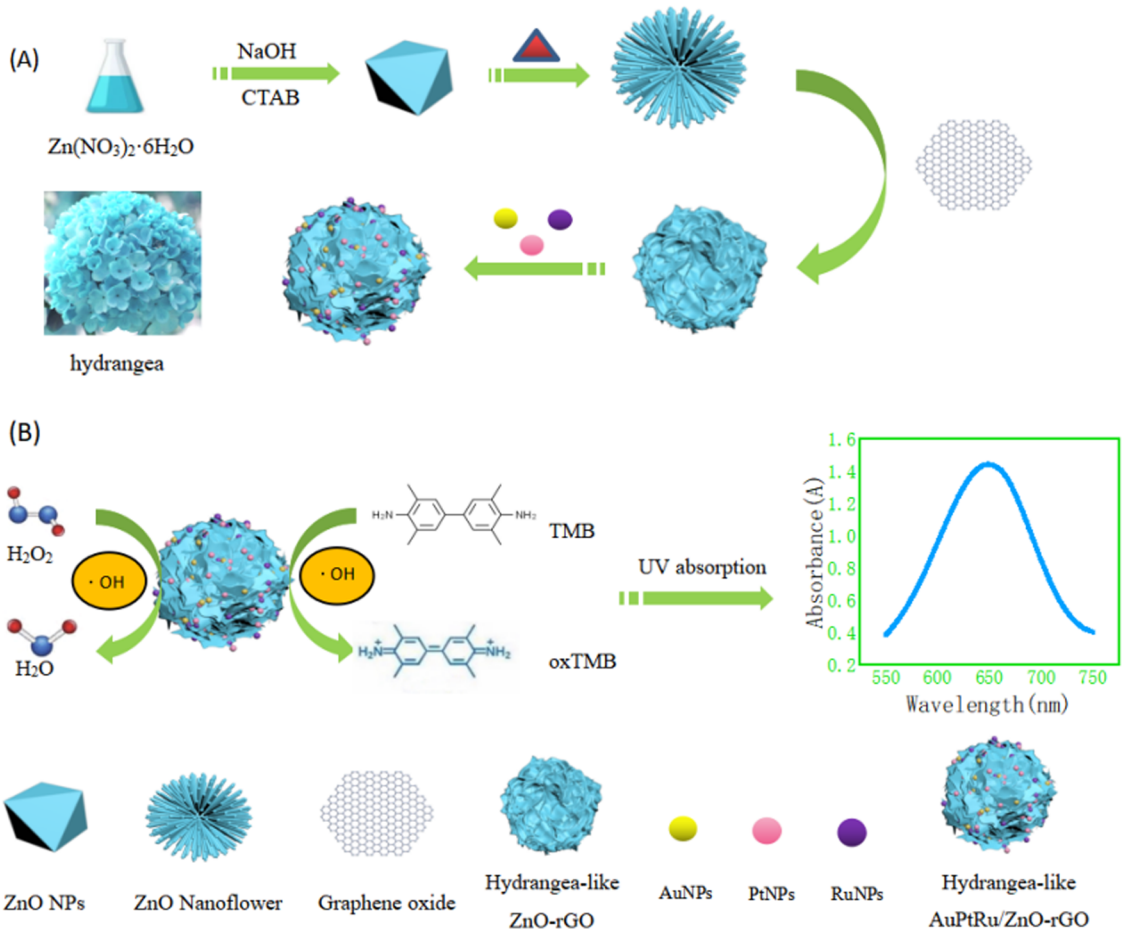

and it has emerged as an important and common method for H_2O_2 detection in recent years.[6] While horseradish peroxidase (HRP), a natural peroxide catalytic enzyme, exhibits efficient catalytic effects within organisms,[7] many certain limitations have been identified in comparison to nanoenzymes, such as high production costs, rigorous preservation conditions, and demanding experimental requirements.[8] Up to now, several techniques have been employed for H_2O_2 detection, such as chromatography,[9] fluorescence,[10] chemiluminescence,[11] and electrochemical methods.[12] Among these, the electrochemical method offers ultrasensitive detection capabilities. Zhang et al.[13] synthesized AuPt/MOF-GrapHene nanozyme for the electrochemical detection of H_2O_2, demonstrating a low detection limit of 19 nmol/L. Although the electrochemical method has excellent detection sensitivity, it can be easily affected by interfering substances during the detection process, leading to unstable experimental results. In contrast, the colorimetric method not only has the advantages of simple operation and intuitive results but also has relatively stable experimental results and higher repeatability. Wang et al.[14] synthesized a 3D V_2O_5-MoS_2/rGO nanocomposite to detect H_2O_2 with a linear range of 20−800 μM and a detection limit of 12.4 μM. Gao et al.[6] prepared molybdenum disulfide nanosheets (MoS_2 NSs) for the colorimetric detection of H_2O_2 by hydrothermal synthesis, with a linear range of 10−50 μM and a detection limit of 1.0 μM, and detected H_2O_2 in milk, the standard addition recovery rate was 92.4−106.9%. Sun et al.[15] coupled molybdenum disulfide and gold nanoparticles to synthesize MoS_2/C-Au nanocomposites, which enhanced the peroxidase-like catalytic activity of molybdenum disulfide and detected H_2O_2 by colorimetry, linear The linear range is 0.01−0.2 mM, and the detection limit is 1.82μM. Colorimetric detection of H_2O_2 has the advantages of intuitive results and easy operation. In terms of practical application, Nghia Duc Nguyen et al.[16] prepared a colorimetric detection card based on AgNPs/GQDs nanocomposites to realize on-site detection, which greatly facilitates the detection of H_2O_2. The practical application of H_2O_2 detection is of great significance.

Metal nanoparticles such as gold and platinum exhibit favorable peroxidase activity, but their lack of spatial structure often leads to stacking issues, resulting in a decrease in active sites. To overcome this limitation, metal nanoparticles are combined with a three-dimensional structure substrate to achieve a synergistic effect[13] and enhance the peroxide catalytic activity of the nanocomposite. One example of such a structured substrate is flower-like ZnO, which possesses a desirable 3D spatial arrangement.[17] This unique morphology can not only provide a larger specific surface area for more active sites but also enable effective binding of metal nanoparticles, particularly using extended prismatic ZnO nanorods.[18] Xia et al.[19] successfully synthesized platinum cubes with a spatial structure (PVP55-Pt) by combining platinum with PVP55, whose peroxidase catalytic activity was

https://doi.org/10.1021/acsomega.3c07499
ACS Omega 2023, 8, 49218−49227

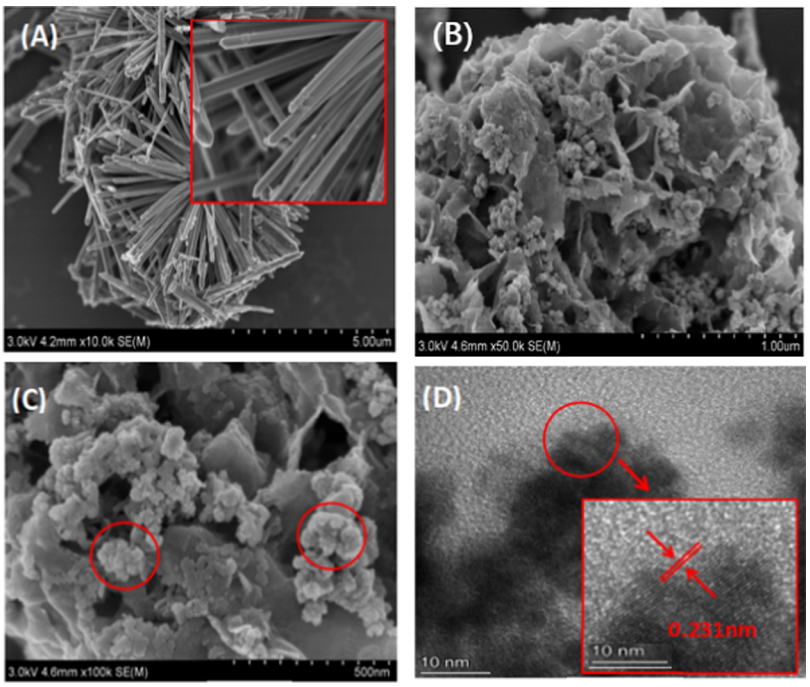

Figure 1. SEM of (A) flower-like ZnO, (B) hydrangea-like ZnO-rGO, (C) hydrangea-like AuPtRu/ZnO-rGO, and (D) TEM of hydrangea-like AuPtRu/ZnO-rGO.

improved by about 200% compared with that of platinum nanoparticles (PtNPs) alone.

In this study, zinc nitrate hexahydrate ($Zn(NO_3)_2{\cdot}6H_2O$), NaOH, cetyltrimethylammonium bromide (CTAB), and reduced graphene oxide (rGO) were used as precursors. Zinc oxide nanoflowers (flower-like ZnO) were synthesized by a one-step hydrothermal method, and gold nanoparticles (AuNPs), platinum nanoparticles (PtNPs), and ruthenium nanoparticles (RuNPs) were loaded by a reduction method,[20] and gold platinum ruthenium was finally synthesized. As shown in Scheme 1, trimetallic zinc oxide nanoflower composite material (AuPtRu/ZnO-rGO), the nanozyme, has good stability and specificity and can be used for sensitive colorimetric detection of H_2O_2.

2. MATERIALS AND METHODS

2.1. Apparatus. A UV-1750 ultraviolet−visible spectrophotometer was provided by Shimadzu, Japan, and an F-4700 fluorescence spectrophotometer was bought from Hitachi Scientific Instruments (Beijing) Co., Ltd.

2.2. Reagents and Materials. Zinc nitrate hexahydrate ($Zn(NO_3)_2{\cdot}6H_2O$), NaOH, and poly(vinylpyrrolidone) (PVP) were purchased from Shanghai Macklin Biochemical Technology Co., Ltd.; hydrogen tetrachloroaurate(III) trihydrate ($HAuCl_4{\cdot}3H_2O$), chloroplatinic acid hexahydrate ($H_2PtCl_6{\cdot}6H_2O$), ruthenium chloride ($RuCl_3$), reduced graphene oxide (Reduced GrapHene-oxide), TMB, 30% H_2O_2, acetate buffer, terephthalic acid (TerepHthalic acid, TA), glycine (Glycine), and glucose (Glucose) were purchased from Shanghai Aladdin Biochemical Technology Co., Ltd.; cetylmethyltrimethylammonium bromide (CTAB) was purchased from Nanjing Chemical Reagent Co., Ltd.; sodium borohydride ($NaBH_4$) was purchased from Tianjin Kemiou Chemical Reagent Co., Ltd.; sodium chloride, magnesium chloride, and potassium chloride were purchased from Chengdu Kelong Chemical Reagent Factory.

2.3. Synthesis of Flower-like ZnO-rGO. Three-dimensional flower-like ZnO nanostructures self-assembled from nanorods were prepared by low-temperature hydrothermal synthesis.[17] Zinc nitrate hexahydrate (1.16 g), 1.6 g of sodium hydroxide, and 0.5 g of cetyltrimethylammonium bromide were dissolved in 35 mL of high-purity water, followed by magnetic stirring for 20 min. Then, 1 mL of reduced graphene oxide (1.0 mg/mL) that had been ultrasonically dispersed for 1 h in advance was added to the above solution, and magnetic stirring was continued for 45 min to form a black solution. Then, the above mixed solution was poured into a 50 mL polytetrafluoroethylene lined tube and sealed; then, the sealed lined tube was put into a muffle furnace and kept warm at 90 °C for 16 h.

Naturally cool to room temperature with the furnace, wash the precipitate with deionized water several times (3000 rpm for 10 min), and finally place the precipitate at 65 °C for 12 h in a vacuum to obtain a white three-dimensional flower-like ZnO-rGO powder.

2.4. Synthesis of Hydrangea-like AuPtRu/ZnO-rGO, Au/ZnO-rGO, Pt/ZnO-rGO, Ru/ZnO-rGO, AuPt/ZnO-rGO, AuRu/ZnO-rGO, and PtRu/ZnO-rGO. Thirty milligrams of the prepared ZnO-rGO dissolved in 20 mL of ultrapure water was taken and ultrasonically dispersed for 30 min. Then, 0.1 g of PVP, 5 mL of 15 mM ruthenium trichloride ($RuCl_3$), 5 mL of 15 mM tetrachloroauric acid ($HAuCl_4$), 5 mL of 15 mM chloroplatinic acid (H_2PtCl_6) were added and the mixture was stirred for 10 min. Then, 3 mL of 1.9 M cold and freshly prepared sodium borohydride ($NaBH_4$) was slowly added dropwise to the above solution and stirred for 90 min. Afterward, the precipitate was centrifuged and washed several times with deionized water (12,000 rpm for 10 min); finally, the precipitate was vacuum-dried at 80 °C for 10 h. Finally, black AuPtRu/ZnO-rGO powder was obtained. Other nanomaterials are synthesized following the aforementioned

https://doi.org/10.1021/acsomega.3c07499
ACS Omega 2023, 8, 49218−49227

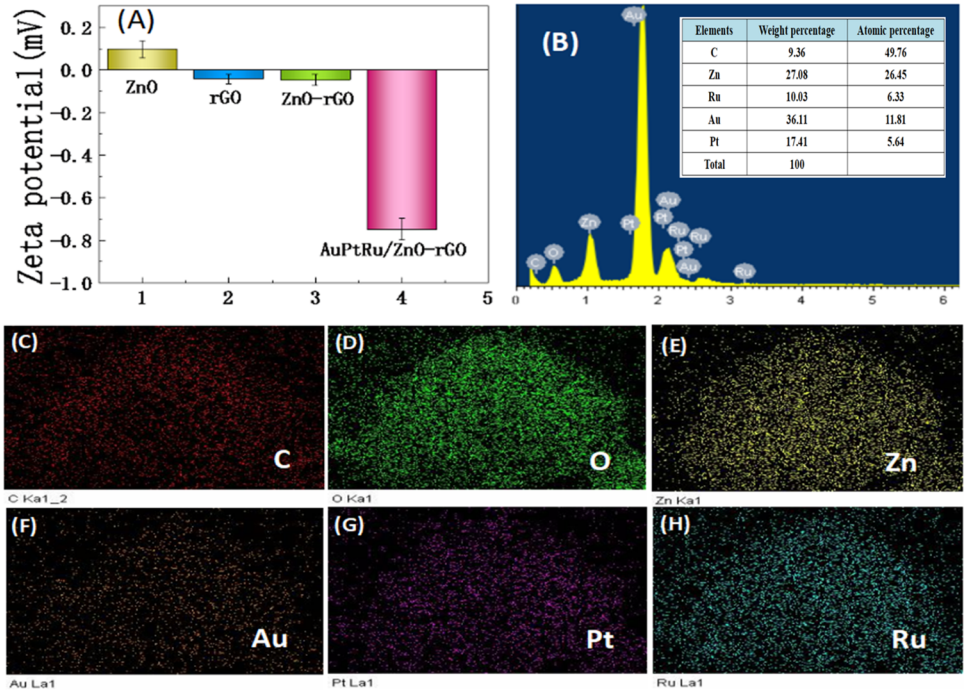

Figure 2. (A) Evolution of zeta potential of ZnO, rGO, ZnO-rGO, and AuPtRu/ZnO-rGO and (B−H) the corresponding elements, C, O, Zn, Au, Pt, Ru of hydrangea-like AuPtRu/ZnO-rGO.

method but only incorporating the respective metallic nanoparticles.

2.5. Catalytic Mechanism Study. After AuPtRu/ZnO-rGO catalyzes the generation of hydroxyl radicals ($^{\bullet}OH$) through the catalysis of H_2O_2 to oxidize TMB, there is an alteration in the valence state of the nanoparticles. The catalytic mechanism is explored by analyzing the variations in zerovalent metallic nanoparticles before and after the catalytic process using XPS spectroscopy. Moreover, terephthalic acid (TA) is employed as a fluorescent probe to validate the production of hydroxyl radicals.

2.6. Analysis of the Steady-State Kinetics. Steady-state kinetic analysis was performed using 50 μL of (2 mg/mL) AuPtRu/ZnO-rGO and 50 μL of (6 mM) TMB in 2 mL of (0.1 mol/L) NaAc-HAc (pH 4.0) buffer solution. By changing the concentration of H_2O_2 (range of 0.05−1.6 mM), measure The absorbance value of the system at 652 nm in the first 0.8 min after the start of the reaction is calculated according to the Lambert−Beer theorem, and the Michaelis constant can be calculated from the Lineweaver−Burk double reciprocal curve,[21] as outlined below:

$$V = \frac{V_{max}[S]}{K_m + [S]}\frac{1}{V} = \frac{K_m}{V_{max}}\frac{1}{[S]} + \frac{1}{V_{max}}$$

2.7. Determination of H_2O_2 Concentration. A series of 5 mL centrifuge tubes were prepared as containers for the reaction system. Then, 2.5 mL of NaAc-HAc (pH 4.0) buffer solution, 50 μL of 2 mg/mL AuPtRu/ZnO-rGO, 50 μL of 6 mM TMB solution, and 100 μL of H_2O_2 solution of different concentrations (1−5000 μM) were added and the contents of each tube were mixed thoroughly. The reaction was allowed to proceed at room temperature for 3 min. Measure the absorbance value of the reaction system at a wavelength of 652 nm, and it is recommended to measure each sample at least three times in parallel to ensure the accuracy and reliability of the results.

2.8. Determination of Spiked Recovery in Actual Samples. A 5 mL centrifuge tube was prepared as a container for the reaction system and 0.25 mL of milk and 2.5 mL of NaAc-HAc (pH 4.0) buffer solution were added. The contents were mixed well and allowed to stand for 10 min to allow the components to stabilize. The mixture was centrifuged at 8000 rpm for 10 min to separate the supernatant. Fifty microliters of 2 mg/mL AuPtRu/ZnO-rGO solution and 50 μL of 6 mM TMB solution were added.

3. RESULTS AND DISCUSSION

3.1. Characterization of Hydrangea-like AuPtRu/ZnO-rGO. From the scanning electron microscopy (SEM) images of the prepared ZnO nanomaterials (Figure 1A), it can be seen that the prepared ZnO is in the shape of nanoflowers formed by the aggregation of numerous ZnO nanorods at one end. Figure 1B shows that sheet-like graphene is combined with the ZnO nanorods, resulting in a ZnO-rGO composite with a hydrangea-like overall shape with a diameter of about 2 μm. As shown in Figure 1C, the trimetallic nanoparticles are observed to agglomerate to form metal nanoclusters, with an average size of 40 nm, which are densely immobilized on the ZnO-rGO observed under a high-power microscope. The TEM image in Figure 1D confirms that AuPtRuNPs are highly dispersed on ZnO-rGO without isolated NPs. Also, the high-resolution TEM image of a single nanoparticle displays distinct lattice fringes with a spacing of 0.231 nm, which is attributed to the face-centered type (fcc-type) AuPtRu(111) planes with 0.235 nm spacing for Au(111) and 0.226 nm spacing for Pt(111) and 0.206 nm spacing for Ru(111).[22−24]

As shown in Figure 2A, it can be observed that the positive charge of ZnO decreased from 0.0982 to −0.0464 mV after being covered with rGO(−0.0416 mV); with the load of electronegative Au, Pt, and Ru NPs, the zeta potential of the

https://doi.org/10.1021/acsomega.3c07499
ACS Omega 2023, 8, 49218−49227

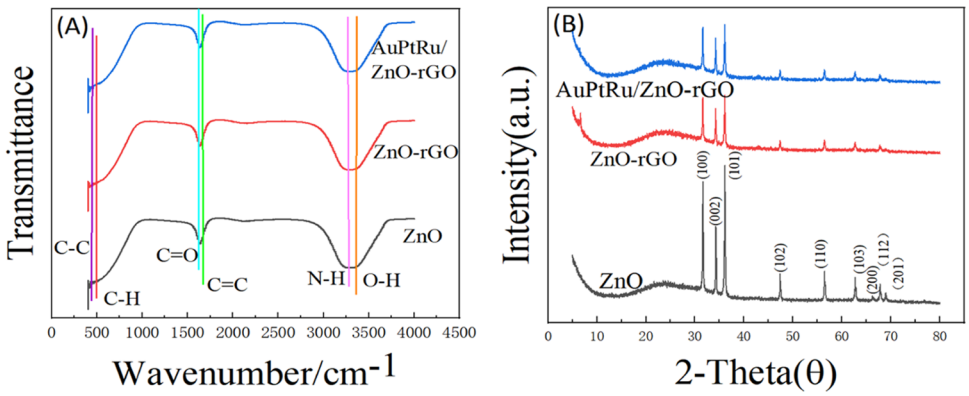

Figure 3. (A) FT-IR spectra and (B) XRD spectra of ZnO, ZnO-rGO, and AuPtRu/ZnO-rGO.

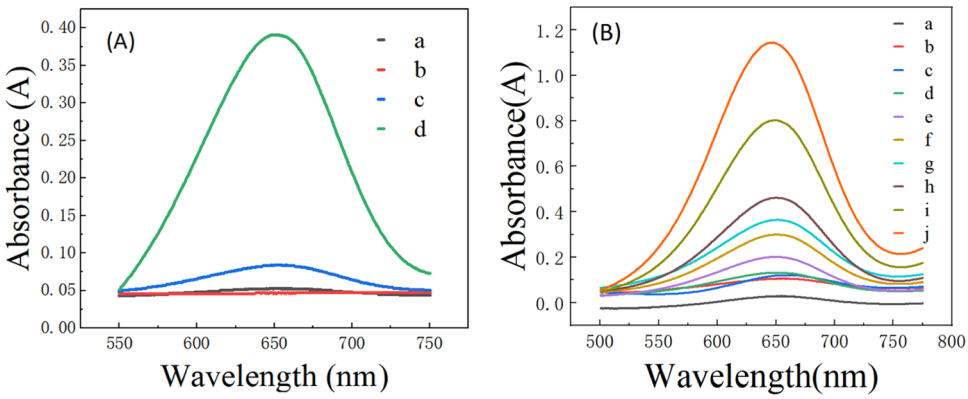

Figure 4. (A) UV−vis absorption spectra of AuPtRu/ZnO-rGO + H_2O_2 + TMB system (a: H_2O_2 + TMB; b: H_2O_2 + AuPtRu/ZnO-rGO; c: TMB + AuPtRu/ZnO-rGO; d: AuPtRu/ZnO-rGO + H_2O_2 + TMB). (B) Comparison of catalytic activities of prepared nanomaterials (a: ZnO; b: rGO; c: ZnO-rGO; d: Au/ZnO-rGO; e: Pt/ZnO-rGO; f: Ru/ZnO-rGO; g: AuPt/ZnO-rGO; h: AuRu/ZnO-rGO; i: PtRu/ZnO-rGO; j: AuPtRu/ZnO-rGO).

nanocomposites become more electronegative (Figure S1). The elemental scanning results depicted in Figure 2B−H show that the nanocomposites predominantly contain Zn, O, C, Au, Pt, and Ru. These elements are uniformly distributed throughout the nanocomposite structure, indicating a homogeneous distribution of the constituents.

As shown in Figure 3A, it can be observed that the three materials exhibit almost the same functional groups. The FT-IR bands at 450−500 cm^{-1} were assigned to the C−C and C−H stretching vibrations, the bands at 1635 and 1645 cm^{-1} were assigned to the C = O and C = C stretching vibration, respectively, C = C in ZnO attributed to Materials Used in Synthesis, FT-IR bands at 3310 and 3410 cm^{-1} were assigned to the N−H and O−H stretching vibrations respectively. The loading of graphene and metal nanoparticles did not change the composition or structure of functional groups. Figure 3B shows the XRD patterns of different nanomaterials obtained. It can be seen from Figure 3B that the diffraction peak shapes of the three materials are basically the same. There are nine groups of characteristic diffraction peaks, and their diffraction positions are consistent with the peak data of the hexagonal fiber mineral standard card (JCPDS NO. 36-1451), also corresponding to the (100), (002), (101), (102), (110), (103), (200), (112), and (201) crystal planes of ZnO. Since the added graphene content is very small, which exceeds the detection sensitivity range of the instrument, no diffraction peaks of graphene were found, but the peak heights decreased after loading graphene and metal nanoparticles.

3.2. Synergistic Effect of Trimetallic to Enhance the Activity of Peroxidases and Catalytic Mechanism of Hydrangea-like AuPtRu/ZnO-rGO. Figure 4A depicts the ultraviolet absorption spectra of the reaction system with different components under the same conditions. In the presence of H_2O_2 + TMB, H_2O_2 + nanozyme, or TMB + nanozyme separately, the absorbance value can hardly be measured at the wavelength of 652 nm, only when H_2O_2, TMB, and nanozyme coexist in the system, a color reaction can occur, resulting in a measurable absorbance value at 652 nm. Figure 4B shows the UV absorption spectrum of ZnO-rGO supported by different metal nanoparticles under the same conditions. When the three metal nanoparticles of Au, Pt, and Ru are loaded on ZnO-rGO separately or in pairs, different degrees of blue color are produced, and different absorbance values are measured at a wavelength of 652 nm (Ru > Pt > Au). The deepest blue color and the highest absorbance value at 652 nm are obtained when all three metal nanoparticles are loaded onto ZnO-rGO simultaneously. Figure 4B demonstrates that Au, Pt, and Ru metal nanoparticles exhibit certain peroxidase activity individually. However, a synergistic effect is observed when all three metal nanoparticles are present simultaneously, resulting in a significant enhancement of peroxidase activity.

To gain a better understanding of the catalytic mechanism, XPS spectra were utilized to examine the changes in the valence states of the elements. The changes in the zero-valence metal nanoparticles before and after the reaction are shown in

https://doi.org/10.1021/acsomega.3c07499
ACS Omega 2023, 8, 49218−49227

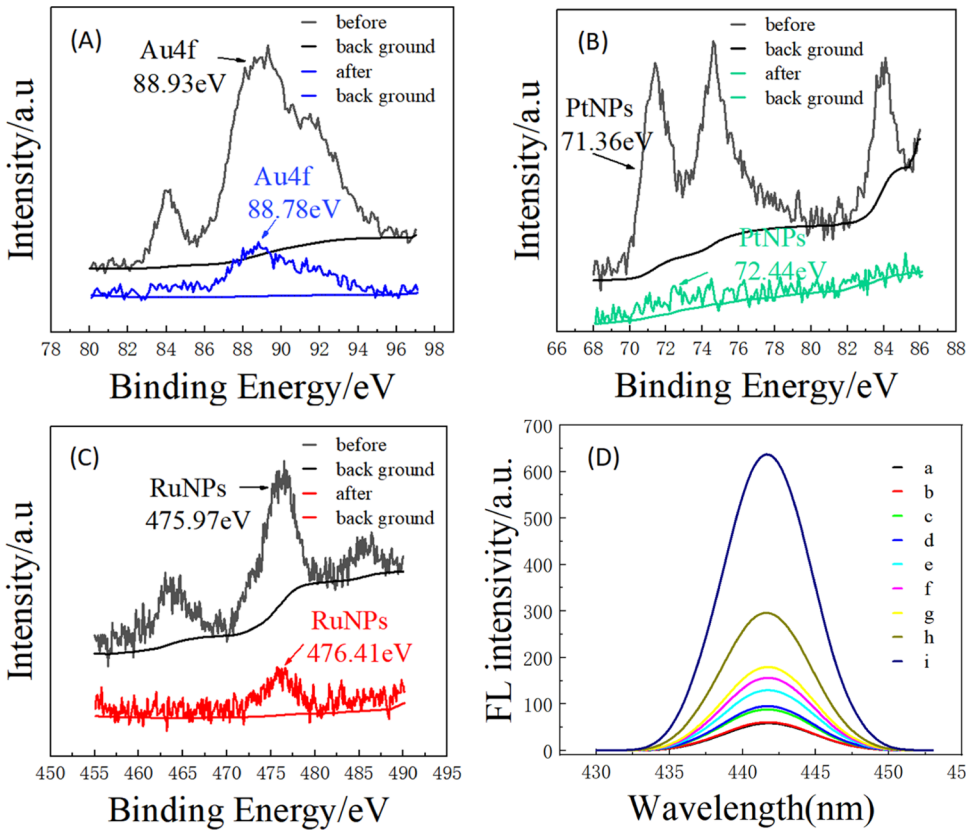

Figure 5. (A–C) High-resolution XPS spectra of Au 4f, Pt 4f, and Ru 3p before and after reaction. (D) Formation of hydroxyl radical (.OH) was identified by fluorescence spectra with terephthalic acid (TA) as a probe (a: TA; b: TA + H_2O_2; c: TA + H_2O_2 + Au/ZnO-rGO; d: TA + H_2O_2 + Pt/ZnO-rGO; e: TA + H_2O_2 + Ru/ZnO-rGO; f: TA + H_2O_2 + AuPt/ZnO-rGO; g: TA + H_2O_2 + AuRu/ZnO-rGO; h: TA + H_2O_2 + PtRu/ZnO-rGO; i: TA + H_2O_2 + AuPtRu/ZnO-rGO) and 100 μL of H_2O_2 solutions of different concentrations (5/200/1000 μM) and mixing the contents of the tube thoroughly and allowing the reaction to proceed at room temperature for 3 min. The absorbance value of the reaction system at a wavelength of 652 nm was measured, and each sample was measured at least three times in parallel.

Figure 5A–C and Table 1. It is observed that the peak area and atomic state proportion of the three elemental metal

Table 1. High Deconvolution of Au 4f, Pt 4f, and Ru 3p of AuPtRu/ZnO-rGO before and after Reaction

	before reaction			after reaction		
peak	peak position (eV)	area (CPS.eV)	actomic (%)	peak position (eV)	area (CPS.eV)	atomic (%)
Au 4f	88.93	9637.72	1.74	88.78	2351.23	0.21
Pt 4f	71.36	4066.21	0.91	72.44	496.58	0.05
Ru 3p	475.97	10842.86	3.43	476.41	4588.91	0.71

nanoparticles decrease after the reaction. These changes in the valence states can be attributed to electron transfer during the catalytic decomposition of hydrogen peroxide.

$$Au + 2H_2O_2 + 2H^+ \rightarrow Au^{2+} + 2\,^{\bullet}OH + 2H_2O \quad (1)$$

$$Pt + 4H_2O_2 + 4H^+ \rightarrow Au^{4+} + 4\,^{\bullet}OH + 4H_2O \quad (2)$$

$$Ru + 2H_2O_2 + 2H^+ \rightarrow Ru^{2+} + 2\,^{\bullet}OH + 2H_2O \quad (3)$$

$$^{\bullet}OH + TMB \rightarrow ox\,TMB \quad (4)$$

To further confirm the production of hydroxyl radicals ($^{\bullet}OH$), terephthalic acid (TA) was employed as a probe molecule.[25] TA reacts with hydroxyl radicals to generate fluorescent hydroxyterephthalic acid (HTA).[26] The fluorescence emission band is 440 nm at an excitation wavelength of 315 nm. Figure 5D describes the fluorescence emission intensity for different nanozymes; among several nanozymes, AuPtRu/ZnO-rGO exhibits the highest fluorescence emission intensity, indicating that the nanocomposite enhanced the decomposition of H_2O_2.

3.3. Optimization of Experimental Conditions. The effect of the reaction conditions on the oxidation of TMB by H_2O_2 catalyzed by AuPtRu/ZnO-rGO was investigated. As shown in Figure 6A, the absorbance value increases with the increase in reaction time. When the reaction time reaches about 5 min, the absorbance value reaches the maximum. Subsequently, the absorbance gradually decreases, indicating that the optimal reaction time for the system is around 5 min. Figure 6B shows the effect of pH on the color reaction of the system. First, the absorbance gradually increases with the increase of pH. When the pH is 4.0, the absorbance reaches the maximum value, and as the pH continues to increase, the absorbance value gradually decreases. This suggests that the system exhibits the most pronounced reaction in a weakly acidic environment, with a pH of 4.0 selected as the optimum pH for the reaction. Figure 6C shows the effect of temperature on the color reaction of the system; in the beginning, the absorbance increases rapidly with the rising temperature; however, the rate of absorbance increase noticeably decreases after 37 °C. Taking into account practical reaction conditions and experimental cost, room temperature is chosen as the

https://doi.org/10.1021/acsomega.3c07499
ACS Omega 2023, 8, 49218–49227

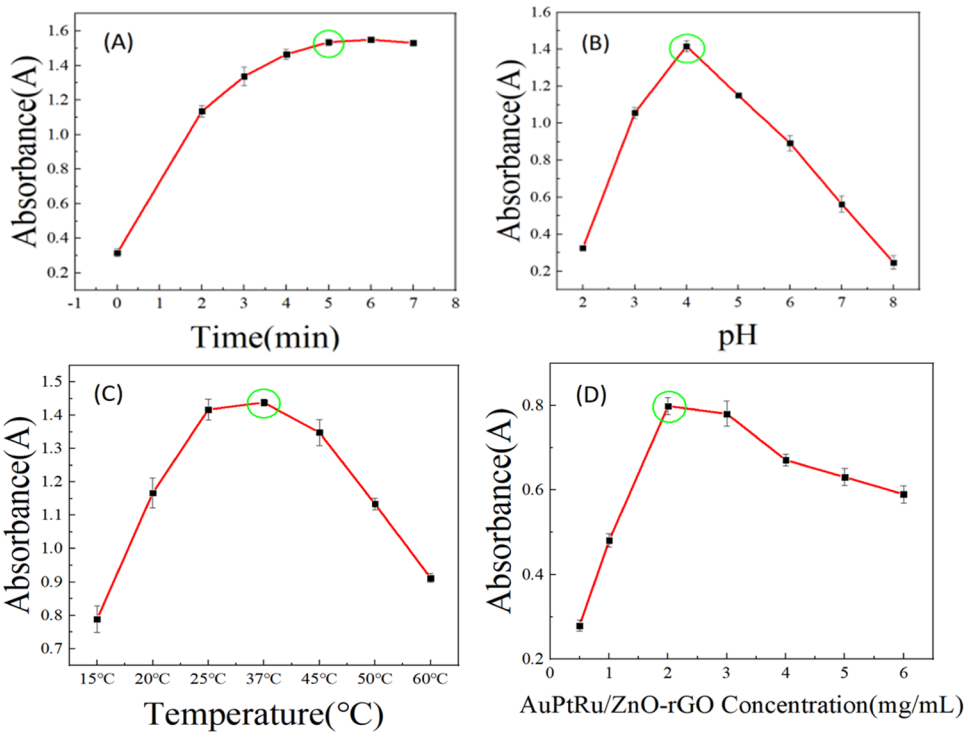

Figure 6. Optimization of (A) time, (B) pH, and (C) temperature in the detection of H_2O_2.

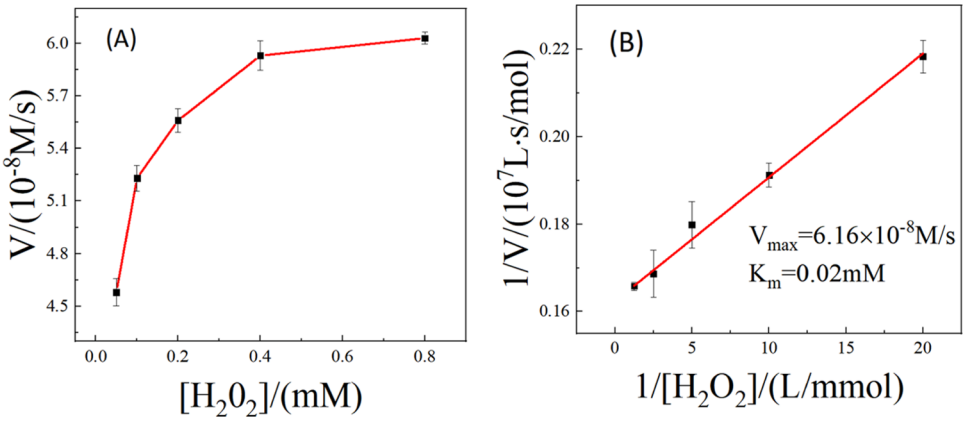

Figure 7. Steady-state kinetic analysis using the Michaelis−Menten model (A) and the Lineweaver−Burk model (B) for hydrangea-like AuPtRu/ZnO-rGO nanocomposites. The concentration of TMB was 6 mM, and the H_2O_2 concentration varied (0.05−0.8 mM).

optimal reaction temperature for the system. As shown in Figure 6D, different concentrations of AuPtRu/ZnO-rGO (0.5, 1, 2, 3, 4, 5, 6 mg/mL) were added into the reaction system; initially, the absorbance increased with increasing concentration. When the concentration exceeded 2 mg/mL, the absorbance began to decrease, and it was observed that the blue color of the system began to turn green; therefore, the optimal concentration of AuPtRu/ZnO-rGO for the detection of H_2O_2 is determined to be 2 mg/mL.

3.4. Analysis of the Steady-State Kinetics. The steady-state kinetic parameters were verified by changing the concentration of H_2O_2. The value ε = 39000 M^{-1} cm^{-1} (at 652 nm) for the oxidized product of TMB was used here to obtain the corresponding concentration term from the absorbance data. Typical Michaelis−Menten curves are shown in Figure 7, and the maximum initial velocity (V_{max}) and Michaelis−Menten constant (K_m) calculated using the Lineweaver−Burk plot are given in Table 2. Compared with horseradish peroxidase (HRP) and other nanozymes, the K_m value of AuPtRu/ZnO−rGO with H_2O_2 as the substrate is lower, indicating a higher catalytic activity of AuPtRu/ZnO−rGO.

Table 2. Comparison of the K_m and V_{max} of Hydrangea-like AuPtRu/ZnO-rGO with HRP and Other Nanozymes

	K_m (mM)	V_{max} (10^{-8} M/s)	
catalyst	H_2O_2	H_2O_2	refs
HRP	3.70	8.71	25
$MgFe_2O_4$ MNPs	4.61	13.46	26
3D V_2O_5-MoS_2/rGO	1.49	0.21	27
MoS_2 NSs	0.1	1.9	28
AuPtRu/ZnO-rGO	0.02	6.16	this work

https://doi.org/10.1021/acsomega.3c07499
ACS Omega 2023, 8, 49218−49227

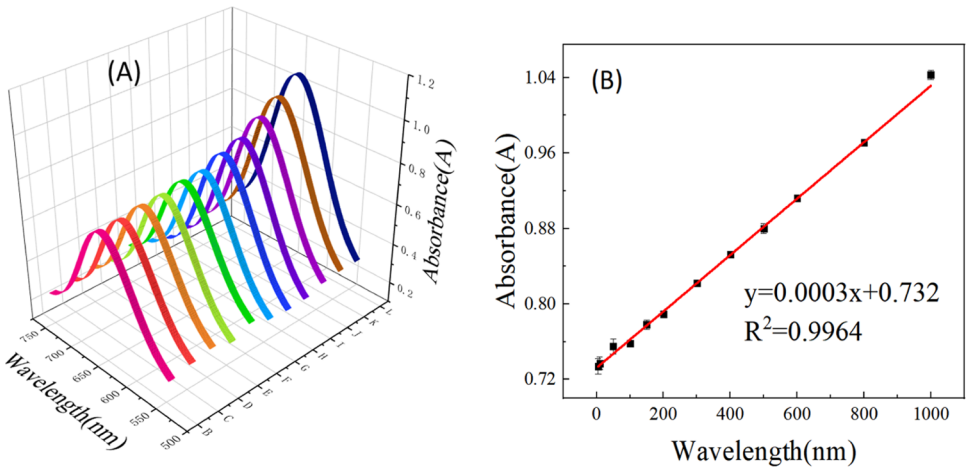

Figure 8. (A) UV−vis absorption spectra of the hydrangea-like AuPtRu/ZnO-rGO-TMB-H_2O_2 system in the presence of different concentrations of H_2O_2 (1−5000 μM). (B) Linear calibration curve for the determination of H_2O_2.

Table 3. Comparison of Colorimetry Results of H_2O_2 Detection

no.	material	method	linear range (μmol/L)	detection limit (μmol/)	refs
1	aniline-co-anthranilic acid	colorimetry	25−500	35.60	29
2	3D V_2O_5-MoS_2/rGO	colorimetry	20−800	12.40	14
3	Ag-Pt/rGO	colorimetry	10−100 and 100−1000	0.9	30
4	MoS_2/ppy nanocomposite	colorimetry	20−2000	45	31
5	nitrogen-doped graphene quantum dots (N-GODs)	colorimetry	20−1170	5.3	32
6	2D ultrathin nanosheets of Co/A1	colorimetry	10−200	10	33
7	AuPtRu/ZnO-rGO	colorimetry	5−1000	3.0	this work

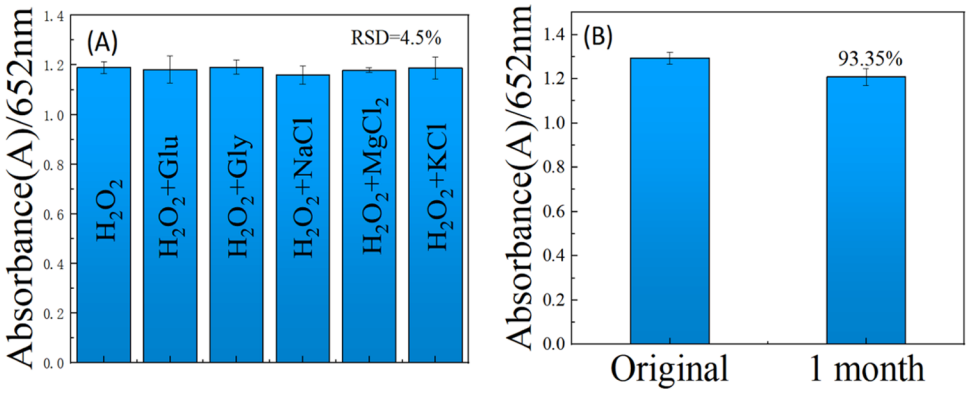

Figure 9. (A) Selective of the hydrangea-like AuPtRu/ZnO-rGO-TMB-H_2O_2 system. The concentration of H_2O_2 and other substances (Glucose, DA, Gly, NaCl, $MgCl_2$, KCl) is 5 mM, RSD (DA) = 4.5% (<5%). (B) Stability of the hydrangea-like AuPtRu/ZnO-rGO-TMB-H_2O_2 system. After one month, the catalytic efficiency of nanoenzyme remained above 93.35%.

3.5. Detection of H_2O_2 with FL-Hydrangea-like AuPtRu/ZnO-rGO. Hydrangea-like AuPtRu/ZnO-rGO-based colorimetric detection was used to detect different concentrations of H_2O_2 under optimal catalytic conditions. Figure 8A shows the ultraviolet absorption spectrum of the reaction system in the presence of different concentrations of H_2O_2 (1−5000 μM). Figure 8B shows a linear relationship between H_2O_2 concentration and absorbance values in the concentration range of 5−1000 μM, with a linear equation of $A = 0.0003C + 0.732$ ($R^2 = 0.9964$) and a detection limit of 3.0 μM (S/N = 3) (LOD is calculated in the Supporting Information). This method has a wide linear range and a lower detection limit compared to other H_2O_2 concentrations (Table 3).

3.6. Stability and Selectivity of Hydrangea-like AuPtRu/ZnO-rGO Colorimetric Detection of H_2O_2 Concentration. The selectivity of the AuPtRu/ZnO-rGO colorimetric detection of H_2O_2 concentration is provided in Figure 9A, and it shows the variation in the catalytic performance of AuPtRu/ZnO-rGO after adding different interfering substances. It can be seen from Figure 9A that the absorbance value changed slightly in the presence of interfering substances, and the relative standard deviation (RSD) is determined to be 4.06%, which is less than 5%. Therefore, it can be concluded that interfering substances have negligible effects on the AuPtRu/ZnO-rGO colorimetric detection of the H_2O_2 concentration. Figure 9B shows the ultraviolet absorption spectrum and histogram of the catalytic performance and original catalytic performance of AuPtRu/

https://doi.org/10.1021/acsomega.3c07499
ACS Omega 2023, 8, 49218−49227

ZnO-rGO after being stored at 4 °C for one month. It is observed that the catalytic activity of the nanozyme remains at 93.35% of the original catalytic performance after one month of storage. This indicates that the nanozyme can be stored at 4 °C for an extended period while maintaining a high level of catalytic activity.

3.7. Detection of the H_2O_2 in the Real Samples. To evaluate the applicability of this method for H_2O_2 detection in real samples, the concentration of H_2O_2 in milk was tested. The milk sample was diluted with NaAc-HAc (pH 4.0) solution, which served to minimize the interference caused by the milky white color of milk and the presence of casein in the reaction. The results are summarized in Table 4, indicating that

Table 4. Detection Results of H_2O_2 in Milk (n = 3)

no.	added (μM)	average found (μM)	recovery (%)	RSD (%, n = 3)
1	5	4.65	93.0	3.3
2	200	192.98	96.5	3.3
3	1000	1017.02	101.7	3.2

the recovery rate of H_2O_2 falls within the range of 93.00−101.70%, and the relative standard deviation (RSD) is between 3.2 and 3.3%. These findings demonstrate the accuracy, reliability, and practicality of this method for the precise determination of H_2O_2 content in milk samples.

4. CONCLUSIONS

Hydrangea-like AuPtRu/ZnO-rGO nanocomposites were synthesized through a straightforward one-step hydrothermal and reduction method. Utilizing the peroxidase-like properties of AuPtRu/ZnO-rGO, a colorimetric method was developed for the determination of the H_2O_2 concentration. The method exhibits a broad linear range of 5−1000 μM and a low detection limit of 3.0 μM (S/N = 3). It demonstrates excellent stability, repeatability, and selectivity. To assess its practicality, the method was employed for detecting the H_2O_2 content in milk samples. The recoveries of standard addition ranged from 93.0% to 101.7%, with a relative standard deviation (RSD) of 3.2−3.3%, indicating its good feasibility. Future research can focus on developing corresponding color charts to facilitate on-site quantitative detection, which holds significant practical value.

■ ASSOCIATED CONTENT

Supporting Information

The Supporting Information is available free of charge at https://pubs.acs.org/doi/10.1021/acsomega.3c07499.

Nanoenzymes demonstrate excellent peroxidase activity due to their remarkable electron transfer capability. Analysis of the steady-state kinetics. LOD calculation. The reduction of metal nanoparticles by $NaBH_4$ (PDF)

■ AUTHOR INFORMATION

Corresponding Author

Chaorui Li − *School of Public Health, Chongqing Medical University, Chongqing 400016, China*; Email: crli@cqmu.edu.cn

Authors

Jie Dong − *School of Public Health, Chongqing Medical University, Chongqing 400016, China*; orcid.org/0009-0000-0964-0889

Laixi Zhang − *School of Public Health, Chongqing Medical University, Chongqing 400016, China*

Wei Li − *School of Public Health, Chongqing Medical University, Chongqing 400016, China*

Xin Hu − *School of Public Health, Chongqing Medical University, Chongqing 400016, China*

Anyi Chen − *School of Public Health, Chongqing Medical University, Chongqing 400016, China*

Complete contact information is available at: https://pubs.acs.org/10.1021/acsomega.3c07499

Notes

The authors declare no competing financial interest.

■ ACKNOWLEDGMENTS

This work was supported by the Natural Science Foundation of Chongqing, China (No. cstc2019jcyj-msxmX0121).

■ REFERENCES

(1) Adibhatla, R. M.; Hatcher, J. F. Lipid Oxidation and Peroxidation in CNS Health and Disease: From Molecular Mechanisms to Therapeutic Opportunities. *Antioxid. Redox Signaling* **2010**, *12* (1), 125−169.

(2) Stearns, R.; Freshour, A.; Shen, C. Literature review for applying peroxyacetic acid and/or hydrogen peroxide to control foodborne pathogens on food products. *J. Agric. Food Res.* **2022**, *10*, No. 100442, DOI: 10.1016/j.jafr.2022.100442.

(3) McKeen, L. Introduction to Food Irradiation and Medical Sterilization. *The Effect of Sterilization on Plastics and Elastomers*, 2012; 1−40.

(4) Bopitiya, D.; Christensen, D.; Martin, M.; Zhang, J.; Bennett, L. E. Production of hydrogen peroxide in formulated beverages is associated with the presence of ascorbic acid combined with selected redox-active functional ingredients. *Food Chem.* **2021**, *338*, No. 127947.

(5) Gao, L. Z.; Zhuang, J.; Nie, L.; Zhang, J. B.; Zhang, Y.; Gu, N.; Wang, T. H.; Feng, J.; Yang, D. L.; Perrett, S.; Yan, X. Intrinsic peroxidase-like activity of ferromagnetic nanoparticles. *Nat. Nanotechnol.* **2007**, *2* (9), 577−583.

(6) Gao, X.; Gao, Y. F. Determination of hydrogen peroxide by colorimetric method based on molybdenum disulfide nanozyme *Anal. Chem.* 2022.

(7) Cao, G. X.; Sun, D. X.; Gu, T. T.; Dong, Y. M.; Wang, G. L. Photoswitching enzymatic activity of horseradish peroxidase by graphene oxide for colorimetric immunoassay. *Biosens. Bioelectron.* **2019**, *145*, No. 111707, DOI: 10.1016/j.bios.2019.111707.

(8) Huang, Y. Y.; Ren, J. S.; Qu, X. G. Nanozymes: Classification, Catalytic Mechanisms, Activity Regulation, and Applications. *Chem. Rev.* **2019**, *119* (6), 4357−4412.

(9) Domergue, L.; Cimetière, N.; Giraudet, S.; Hauchard, D. Determination of hydrogen peroxide by differential pulse polarography in advanced oxidation processes for water treatment. *J. Water Process Eng.* **2023**, *53*, No. 103707, DOI: 10.1016/j.jwpe.2023.103707.

(10) Ma, T.; Fu, K.; Li, Z. C.; Yuan, C. C.; Ma, W. B. A novel hydrogen peroxide fluorescent probe for bioimaging detection and enables multiple redox cycles. *Spectrochim. Acta, Part A* **2022**, *276*, No. 121218, DOI: 10.1016/j.saa.2022.121218.

(11) Song, Y.; Wang, C. T.; Sha, J. C.; Liu, X. Y.; Han, L. X.; Li, L. Photoelectrochemical sensor based on the sensitive interface of photosensitive electrode for the detection of hydrogen peroxide in dried bean curds. *J. Food Compos. Anal.* **2023**, *119*, No. 105237, DOI: 10.1016/j.jfca.2023.105237.

(12) Xing, L. J.; Zhang, W. G.; Fu, L. J.; Lorenzo, J. M.; Hao, Y. J. Fabrication and application of electrochemical sensor for analyzing hydrogen peroxide in food system and biological samples. *Food Chem.* **2022**, *385*, No. 132555, DOI: 10.1016/j.foodchem.2022.132555.

(13) Zhang, T.; Xing, Y.; Song, Y.; Gu, Y.; Yan, X.; Lu, N.; Liu, H.; Xu, Z.; Xu, H.; Zhang, Z.; Yang, M. AuPt/MOF-Graphene: A Synergistic Catalyst with Surprisingly High Peroxidase-Like Activity and Its Application for H(2)O(2) Detection. *Anal. Chem.* **2019**, *91* (16), 10589−10595.
(14) Wang, D.; Dang, X.; Tan, B.; Zhang, Q.; Zhao, H. 3D V(2)O(5)-MoS(2)/rGO nanocomposites with enhanced peroxidase mimicking activity for sensitive colorimetric determination of H(2)O(2) and glucose. *Spectrochim. Acta, Part A* **2022**, *269*, No. 120750.
(15) Sun, H. H.; Gao, Y.; Hu, N. R. S.; Zhang, Y. X.; Guo, C. S.; Gao, G. G.; Ma, Z.; Ivanovich, K. I.; Qiu, Y. F. Electronic coupling between molybdenum disulfide and gold nanoparticles to enhance the peroxidase activity for the colorimetric immunoassays of hydrogen peroxide and cancer cells. *J. Colloid Interface Sci.* **2020**, *578*, 366−378.
(16) Nguyen, N. D.; Nguyen, T. V.; Chu, A. D.; Tran, H. V.; Tran, L. T.; Huynh, C. D. A label-free colorimetric sensor based on silver nanoparticles directed to hydrogen peroxide and glucose. *Arabian J. Chem.* **2018**, *11* (7), 1134−1143.
(17) Tak, M.; Gupta, V.; Tomar, M. Flower-like ZnO nanostructure based electrochemical DNA biosensor for bacterial meningitis detection. *Biosens. Bioelectron.* **2014**, *59*, 200−207.
(18) Lin, Y. S.; Hu, S. H.; Chen, C. W.; Su, S. H.; Dai, H.; Ai, Y. Z. Establishing a gold nanoparticle quasi-mesh structure in Al-doped zinc oxide film to enhance photoelectric properties. *Vacuum* **2021**, *194*, No. 110557, DOI: 10.1016/j.vacuum.2021.110557.
(19) Ye, H. H.; Liu, Y. Z.; Chhabra, A.; Lilla, E.; Xia, X. H. Polyvinylpyrrolidone (PVP)-Capped Pt Nanocubes with Superior Peroxidase-Like Activity. *ChemNanoMat* **2017**, *3* (1), 33−38.
(20) Wang, L. B.; Ge, S. M.; Gao, C. F.; Yan, H.; Wang, J.; Jia, J. Q.; Wu, Q. Y. One-pot synthesis of gold-copper nanoparticles mediated by silk fibroin peptides: Peroxidase-like properties and its application in antioxidant detection. *Microchem. J.* **2023**, *185*, No. 108250, DOI: 10.1016/j.microc.2022.108250.
(21) Shekhar, S.; Sarker, R.; Mahato, P.; Agrawal, S.; Mukherjee, S. pH-Switchable phenylalanine-templated copper nanoclusters: CO2 probing and efficient peroxidase mimicking activity. *Nanoscale* **2023**, *15*, 15368−15381, DOI: 10.1039/D3NR04195F.
(22) Lee, S. B.; Kang, S.-G.; Jung, J.; Sung, S.; Yoo, S. J.; Han, H. N. Lattice shear and non-random rotation of Au nanoparticles under electron-beam irradiation. *Acta Mater.* **2022**, *241*, No. 118387, DOI: 10.1016/j.actamat.2022.118387.
(23) Yu, E.; Li, J.; Chen, J.; Chen, J.; Hong, Z.; Jia, H. Enhanced photothermal catalytic degradation of toluene by loading Pt nanoparticles on manganese oxide: Photoactivation of lattice oxygen. *J. Hazard. Mater.* **2020**, *388*, No. 121800.
(24) Zhang, C.; Yin, H.; Bai, X.; Yang, Z. Ru doping induced lattice distortion of Cu nanoparticles for boosting electrochemical non-enzymatic hydrogen peroxide sensing. *Colloids Surf., A* **2023**, *666*, No. 131311, DOI: 10.1016/j.colsurfa.2023.131311.
(25) Zhang, T.; Zhang, S. T.; Liu, J.; Li, J.; Lu, X. Q. Efficient Visual Chemosensor for Hexavalent Chromium via a Controlled Strategy for Signal Amplification in Water. *Anal. Chem.* **2020**, *92* (4), 3426−3433.
(26) Jin, G. X.; Liu, J.; Wang, C.; Gu, W. X.; Ran, G. X.; Liu, B.; Song, Q. J. Ir nanoparticles with multi-enzyme activities and its application in the selective oxidation of aromatic alcohols. *Appl. Catal., B* **2020**, *267*, No. 118725, DOI: 10.1016/j.apcatb.2020.118725.
(27) Tan, Z. L.; Dong, H.; Liu, Q.; Liu, H.; Zhao, P. P.; Wang, P.; Li, Y. Y.; Zhang, D. P.; Zhao, Z. D.; Dong, Y. H. A label-free immunosensor based on PtPd NCs@MoS2 nanoenzymes for hepatitis B surface antigen detection. *Biosens. Bioelectron.* **2019**, *142*, No. 111556, DOI: 10.1016/j.bios.2019.111556.
(28) Xia, C.; Xu, L.; Li, Z.; Guo, L. Sulfur defect-engineered MoS2 nanosheets with enhanced peroxidase-like activity. *Appl. Surf. Sci.* **2023**, *635*, No. 157777, DOI: 10.1016/j.apsusc.2023.157777.
(29) Hosu, O.; Lettieri, M.; Papara, N.; Ravalli, A.; Sandulescu, R.; Cristea, C.; Marrazza, G. Colorimetric multienzymatic smart sensors for hydrogen peroxide, glucose and catechol screening analysis. *Talanta* **2019**, *204*, 525−532.
(30) Yao, L.; Kong, F. Y.; Wang, Z. X.; Li, H. Y.; Zhang, R.; Fang, H. L.; Wang, W. UV-assisted one-pot synthesis of bimetallic Ag-Pt decorated reduced graphene oxide for colorimetric determination of hydrogen peroxide. *Microchim. Acta* **2020**, *187* (7), No. 410, DOI: 10.1007/s00604-020-04350-3.
(31) Lei, J. Y.; Lu, X. F.; Nie, G. D.; Jiang, Z. Q.; Wang, C. One-Pot Synthesis of Algae-Like MoS2/PPy Nanocomposite: A Synergistic Catalyst with Superior Peroxidase-Like Catalytic Activity for H2O2 Detection. *Part. Part. Syst. Charact.* **2015**, *32* (9), 886−892.
(32) Lin, L. P.; Song, X. H.; Chen, Y. Y.; Rong, M. C.; Zhao, T. T.; Wang, Y. R.; Jiang, Y. Q.; Chen, X. Intrinsic peroxidase-like catalytic activity of nitrogen-doped graphene quantum dots and their application in the colorimetric detection of H2O2 and glucose. *Anal. Chim. Acta* **2015**, *869*, 89−95.
(33) Chen, L.; Sun, B.; Wang, X.; Qiao, F.; Ai, S. 2D ultrathin nanosheets of Co-Al layered double hydroxides prepared in l-asparagine solution: enhanced peroxidase-like activity and colorimetric detection of glucose. *J. Mater. Chem. B* **2013**, *1* (17), 2268−2274.

https://doi.org/10.1021/acsomega.3c07499
ACS Omega 2023, 8, 49218−49227